Tuning of spin-orbit coupling in metal-free conjugated polymers by structural conformation

Eric Vetter, 13 Ian VonWald, Shijia Yang, Liang Yan, Sanaz Koohfar, Divine Kumah, Zhi-Gang Yu, 5 Wei You, 2,6,* and Dali Sun, 1,6,†

¹Department of Physics, North Carolina State University, Raleigh, North Carolina 27695, USA ²Department of Chemistry, University of North Carolina at Chapel Hill, Chapel Hill, North Carolina 27599, USA ³Department of Material Science and Engineering, North Carolina State University, Raleigh, North Carolina 27695, USA ⁴ISP/Applied Sciences Laboratory, Washington State University, Spokane, Washington 99202, USA ⁵Department of Physics and Astronomy, Washington State University, Pullman, Washington 99164, USA ⁶Organic and Carbon Electronics Lab (ORaCEL), North Carolina State University, Raleigh, North Carolina 27695, USA

(Received 6 January 2020; accepted 31 July 2020; published 28 August 2020)

Manipulating spin-orbit coupling (SOC) is a key achievement for spin-orbitronic applications since SOC determines spin-diffusion lengths and spin-to-charge conversion efficiencies. While in most organic semiconductors SOC is inherently very weak due to being composed of primarily light elements, the SOC in conjugated polymer systems is also intimately tied to the polymer's structural conformation and thus may be manipulated. Here we report a modification of SOC in conjugated polymers by altering torsion angle between conjugated units. Spin-pumping experiments are performed on three poly(3-alkylthiophene) polymer films with decreasing conjugation lengths and concomitantly increasing torsion angle. The more twisted polymer exhibits a shorter spin-diffusion length and a giant spin-mixing conductance (up to $10^{21} \, \mathrm{m}^{-2}$), which is attributed to an increased SOC by structural conformation. This work offers a route for enhancing SOC and spin-injection efficiency in organic materials for spintronic applications.

DOI: 10.1103/PhysRevMaterials.4.085603

I. INTRODUCTION

Spintronics embodies the concept of utilizing both the spin and charge degrees of freedom of carriers for new devices and applications, whose functions cannot be easily achieved in conventional electronic devices [1]. The recent emergence of novel spintronic studies focuses on the generation, transmission, and control of a "pure spin current" by means of the spin-orbit coupling (SOC) in the material, which enables the conversion of a pure spin current into a charge current or vice versa [2]. This process has initiated a myriad of SOCbased spintronic applications, e.g., spin-to-charge convertors and spin-orbit torque devices, in a variety of materials including heavy metals [3], two-dimensional electron gases [4], topological insulators [5], and inorganic semiconductors [6]. Tailoring SOC is typically achieved via heavy-metal doping [7,8] and is integral to novel Rashba splitting states [9] and topological phases [10].

In order to measure SOC in a wide variety of materials, the spin-pumping technique has emerged as a high-fidelity method for determining SOC-dependent parameters such as the spin Hall angle and spin-diffusion length [11]. Here, microwave excitation is used to drive ferromagnetic resonance (FMR) in a ferromagnetic thin film in the presence of an applied magnetic field, generating a pure spin current in an adjacent material with indeterminate SOC. Additionally, the spin current injected into this SOC material may be converted into a corresponding charge current via the inverse spin Hall effect (ISHE), with the conversion efficiency encapsulated by the spin Hall angle (θ_{SH}) . Parametric studies utilizing both FMR and ISHE as a function of the SOC material's thickness allow for the direct determination of spin-diffusion lengths and spin-to-charge conversion efficiencies, which ultimately relate back to the strength of SOC. This has been well established in a multitude of inorganic materials systems, including both metals and semiconductors [6,12].

Recently, the spin-pumping technique and its usefulness in determining the magnitude of SOC has also been applied to organic systems. Given that organic materials have on average a very low atomic number (Z) owing to the predominance of carbon and hydrogen, and that $\theta_{SH} \propto SOC \propto Z^4$, it might be expected that SOC is generally very weak in organics with concomitantly low spin Hall angles. Indeed, this is borne out by fruitful spin-pumping experiments in organic systems such as PBTTT [13], doped PEDOT:PSS [14], and polyaniline [15], where spin Hall angles are orders of magnitude lower than those in strong SOC heavy metals and spin-diffusion lengths are accordingly orders of magnitude higher. The long spin-diffusion lengths and spin lifetimes in organic materials generally makes them ideal candidates for spin-transport materials. However, not all organic materials follow this trend, with some materials like C_60 [16] and Alq₃ [17] exhibiting surprisingly high SOC on par with that in heavy-metal systems.

Remarkably, there are differences in the nature of SOC in organic solids as compared to inorganic solids. SOC, by

^{*}wyou@unc.edu

[†]dsun4@ncsu.edu

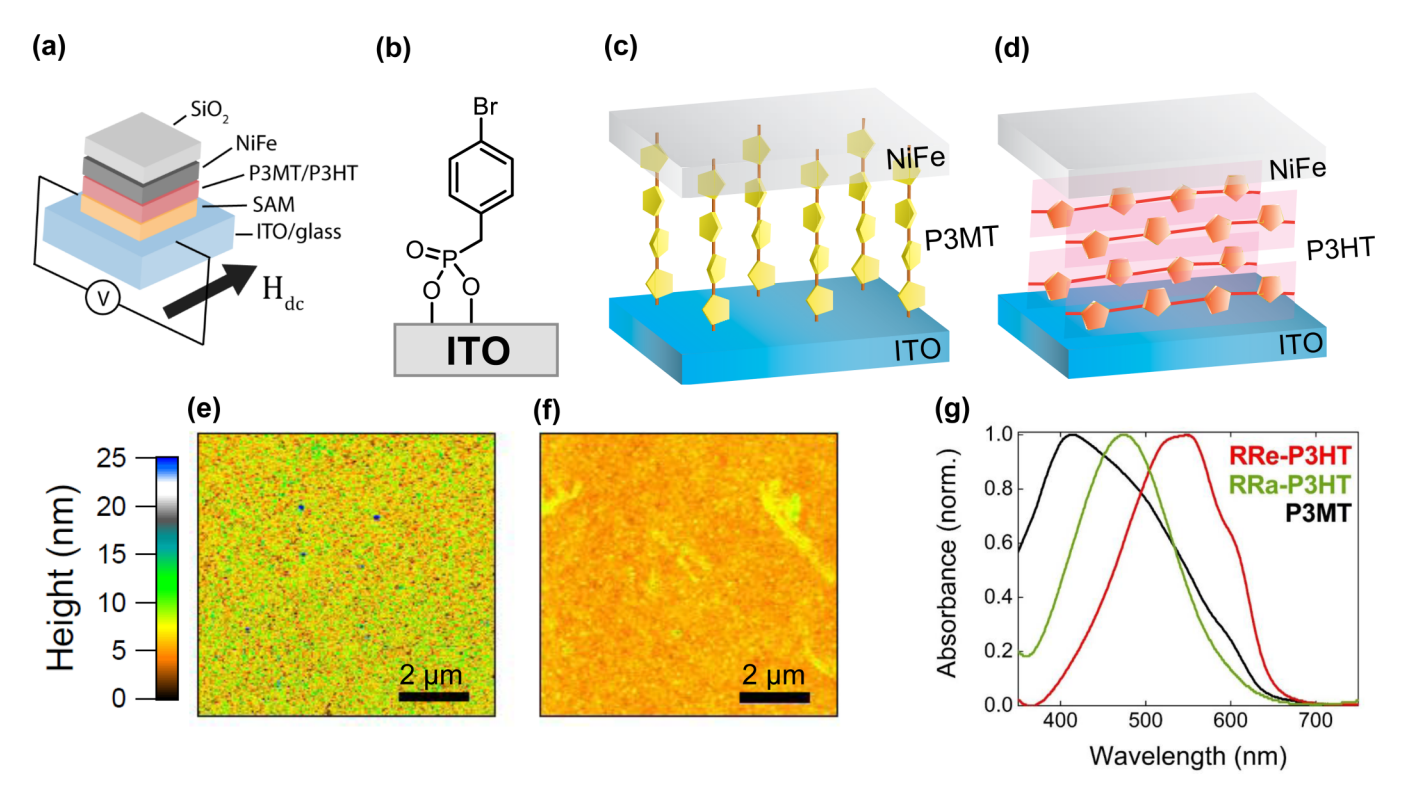


FIG. 1. (a) Schematic representation of device structure. (b) Structure of monolayer used to modify ITO prior to either (c) growth of poly(3-methylthiophene) (P3MT) polymer brush from the monolayer, or (d) deposition of poly(3-hexylthiophene) (P3HT) by spin casting. (e), (f) Respective characterization of P3MT polymer brush (6.3-nm average thickness, rms roughness 2.6 nm) and spin-cast RRe-P3HT (6.5-nm average thickness, rms roughness 0.7 nm) films by AFM. (g) Absorbance spectra for P3MT polymer brush and spin-cast RReP3HT and RRa-P3HT films of 32-nm thickness.

definition, enables the transfer of angular momenta between orbitals and spins, and in organic solids the molecular orbitals are strongly influenced by the materials' structural conformation. Theoretical models for SOC in these cases have been established where a large SOC may be obtained in conjugated organic systems when π orbitals are misaligned [18,19]. This model can be used to explain the aforementioned discrepancies in SOC strength in Alq₃ molecules, where its three conjugated ligands are orthogonally arranged [19], and C_60 , where the curvature of its spherical geometry prevents parallel alignment of the π orbitals [20,21]. Since its recent inception, this model has also been supported experimentally through spin-pumping experiments in conjugated polymers with varying degrees of planarity [13,22,23].

In this work, we experimentally verify that a tailored SOC can be achieved in conjugated polymers through structural conformation by varying the degree of torsion between conjugated units along the polymer backbone of polyalkylthiophenes. The strength of SOC in the "twisted" conjugated polymer is probed by measuring the spin-diffusion length and the effective spin-mixing conductance in a Ni₈₁Fe₁₉/polymer/ITO trilayer heterostructure using a spin-pumping approach, wherein the organic polymer constitutes either a grafted poly(3-methylthiophene) conjugated polymer brush (P3MT, twisted case) or spin-coated poly(3-hexylthiophene) film (P3HT, "planar" case; either regioregular (RRe-P3HT) or regiorandom (RRa-P3HT), defined by the side-chain arrangement). The RRa-P3HT possesses a more twisted conformation

than the RRe-P3HT, with planarization frustrated by the steric hindrance of the randomized side chains.

Through a comparative study of ferromagnetic resonance and ISHE measurements between these three types of polymers at room temperature as a function of polymer thickness, we find that P3MT exhibits a consistently higher spin-mixing conductance and shorter spin-diffusion length than that in P3HT, despite the similarities in their chemical structure and electronic properties. These differences are attributed to a stronger effective SOC in P3MT as a result of the polymer's structural conformation, supported by recent theoretical treatments of SOC and its effects in disordered organic semiconductors [18,19]. Remarkably, we observe a high spin-mixing conductance (up to 10^{21} m⁻²) at the NiFe/P3MT interface that is two orders of magnitude higher than that in conventional inorganic bilayer heterostructures (in the range of 10¹⁸ to 10¹⁹ m⁻²), suggesting a very efficient spin injection at the ferromagnet/polymer interface.

II. EXPERIMENTAL DETAILS

Figure 1(a) shows a schematic of the fabricated device structures consisting of glass substrate/ITO (145 nm)/polymer (d_s) /NiFe (15 nm)/SiO₂ (50 nm), where the polymer layer constitutes a self-assembled monolayer (SAM) on top of the ITO film, followed by a spin-coated P3HT film or grafted P3MT polymer brush layer with thickness d_s , respectively. This trilayer heterostructure design, where an organic

semiconductor is sandwiched between a ferromagnetic top layer and bottom spin-sink layer, allows for the facile measurement of these organic materials despite poor conductivities ($\sigma \approx 10^{-5} - 10^{-7} \text{ S cm}^{-1}$ in undoped polyalkylthiophenes) and mobilities leading to the negligible generation of charge current within their layer, whereas for more conductive polymers (e.g., PEDOT:PSS $\sigma \approx 10^3 \, \mathrm{S \, cm^{-1}}$) a bilayer design may be used for the direct detection of charge current from the polymer [14].

The molecular structure of the SAM is shown in Fig. 1(b), with schematics of the two polymer heterostructures shown in Figs. 1(c) and 1(d), highlighting their structural differences. For SAM preparation, the pretreated ITO substrates (see the method in Supplemental Material, section I [24]) were immersed in a 10 mM solution of (4-bromobenzyl)phosphonic acid in absolute ethanol overnight without stirring. The substrate was quickly dried under a stream of N_2 and annealed in an inert atmosphere at 150 °C overnight. Finally, the substrates were sonicated for several minutes in a 2:1 solution of ethanol/0.5 M aqueous K₂CO₃ to remove any physisorbed material, yielding monolayer-functionalized

Regioregular P3HT (Rieke Metals, $M_n = 20 \,\mathrm{kg/mol}$, [D = 2.24) and regiorandom P3HT (Rieke Metals, $M_n =$ 23 kg/mol, [D = 2.05) were spin cast at various speeds from chlorobenzene solutions of the appropriate concentrations onto monolayer-functionalized ITO substrates. P3MT brushes were synthesized by a surface-initiated Kumada catalyst transfer polycondensation, as described previously [25]. The films were used without annealing and stored in the dark under inert atmosphere (<1 wk). The resulting P3MT polymer brush and spin-cast P3HT film thicknesses were measured using atomic force microscopy (AFM) scratch profilometry [25]. The film thickness was determined from \geq 10 line scans derived from \geq 2 AFM scratch images. Figures 1(e) and 1(f) show representative AFM scans for 6.3-nmthick P3MT and 6.5-nm-thick RRe-P3HT films. It is evident from these images that the P3HT films exhibit a relatively smooth, homogeneous surface while the P3MT films possess a densely packed columnar morphology with polymer columns oriented vertically out of the plane of the film, as we previously observed [25]. Absorbance spectra for 32-nm thick P3MT, RRa-P3HT, and RRe-P3HT films are shown in Fig. 1(g) [24].

The prepared P3MT and P3HT films were directly transferred through a N_2 glovebox without exposure to air for the device fabrication. 15 nm of Ni₈₁Fe₁₉ (99.99% purity, Angstrom Engineering) was deposited on top of the polymer films by e-beam evaporation (base pressure: $\sim 5.0 \times$ 10^{-8} Torr) at room temperature using a shadow mask, followed by a 50-nm SiO₂ (99.99%) capping layer. FMR was performed at room temperature from 2 to 12 GHz using a commercial NanOSC PhaseFMR spectrometer with a coplanar waveguide, and an electromagnet was used for applying in-plane magnetic fields. For ISHE measurements, the microwaves are generated by a Keysight X-Series microwave analog signal generator at an excitation frequency of 9 GHz and microwave power of 50 mW. The ISHE voltage generated across the edges of the sample was measured using an EG&G 7260 DSP lock-in amplifier.

III. RESULTS AND DISCUSSION

A. Ferromagnetic resonance and spin-mixing conductance

Figure 2(a) shows a schematic of the spin-pumping process as well as typical FMR spectra measured at 9 GHz, from which values for α , the damping parameter, γ , the gyromagnetic ratio, and M_s , the saturation magnetization, are obtained. Damping factors are extracted using the relation $\alpha = \frac{\sqrt{3}\gamma}{4\pi f} \Delta H + H_0$ [12], as shown in Fig. 2(b), where ΔH is the FMR linewidth (HWHM) and f is the microwave frequency. H_0 is the frequency-independent linewidth contribution arising from inhomogeneities in the organic film and the ferromagnet. M_s and γ are obtained from the H_{FMR} versus f plots, shown in the inset of Fig. 2(b), by fitting to the Kittel equation: $(\frac{2\pi f}{\gamma})^2 = H_{FMR}(H_{FMR} + 4\pi M_s)$ [26], where H_{FMR} is the resonant field. Values for $4\pi M_s$ and γ for a bare NiFe reference sample are found to be 0.9609 T and 1.85 \times 10¹¹ T⁻¹ s⁻¹, respectively, which are consistent with those reported in literature [12]. The intrinsic damping parameter, α_0 , for the bare NiFe reference sample grown on top of the glass substrate is 7.2×10^{-3} , while the damping parameters of the NiFe/P3MT/SAM/ITO, NiFe/RRe-P3HT/SAM/ITO, NiFe/SAM/ITO, NiFe/ITO samples are equal to 4.8×10^{-2} , 1.8×10^{-2} , 8.7×10^{-3} , and 7.7×10^{-3} , respectively. This enhancement in the damping factor, α , has been attributed to spin-current dissipation across the ferromagnet/organic interface [14,15,23]. Figure 2(c) shows the enhancement of damping factor, $\Delta \alpha = \alpha - \alpha_0$, as a function of organic layer thickness in the NiFe/P3MT and NiFe/P3HT samples, respectively.

For the P3HT samples, $\Delta \alpha$ increases and then saturates as the thickness is increased above 20–30 nm, similar to the behavior observed in ferromagnet/nonmagnetic metal bilayers [3]. For the P3MT samples, however, $\Delta \alpha$ increases at a much higher rate compared to the P3HT samples and exhibits no clear saturation even in the thickest film. We were unable to extract $\Delta \alpha$ from P3MT films with thickness >30 nm due to roughness of the polymer brush film and low peak intensity (see Supplemental Material [24] for further details). The thickness-dependent enhanced damping factors were fit using a traditional spin-pumping model [3]:

$$\Delta \alpha = \frac{\gamma \hbar}{4\pi M d_r} g_{\text{eff}}^{\uparrow\downarrow},\tag{1}$$

$$\Delta \alpha = \frac{\gamma \hbar}{4\pi M_s d_F} g_{\text{eff}}^{\uparrow\downarrow}, \tag{1}$$

$$g_{\text{eff}}^{\uparrow\downarrow} = g^{\uparrow\downarrow} \frac{1}{1 + \left[2\sqrt{\varepsilon/3} \tanh \left(d_s/\lambda\right)\right]^{-1}}, \tag{2}$$

where \hbar , d_F , λ , and $g_{\rm eff}^{\uparrow\downarrow}$ are the Planck constant, ferromagnetic layer thickness, spin-diffusion length of the organic layer, and real part of the spin-mixing conductance, respectively, and $g^{\uparrow\downarrow}$ represents $g_{\text{eff}}^{\uparrow\downarrow}(d_s \to \infty)$. ε is a dimensionless parameter proportional to the product of the atomic number and fine-structure constant in the nonmagnetic material and is fixed at $\varepsilon = 0.1$ (see sec. IV of Supplemental Material [24] for further discussion). We find that for the P3MT samples $\lambda_s = 10.4 \pm 1.1$ nm and $g^{\uparrow\downarrow} = 1.06 \times 10^{21} \pm 5.1 \times 10^{21}$ $10^{19} \mathrm{m}^{-2}$, while for the RRe-P3HT samples $\lambda_s = 15.0 \pm$ 5.4 nm and $g^{\uparrow\downarrow} = 1.92 \times 10^{20} \pm 1.6 \times 10^{19} \,\mathrm{m}^{-2}$ (For RRa-P3HT, $\lambda_s = 11.7 \pm 3.4 \,\text{nm}$ and $g^{\uparrow\downarrow} = 4.22 \times 10^{20} \pm 3.8 \times 10^{20} \times$

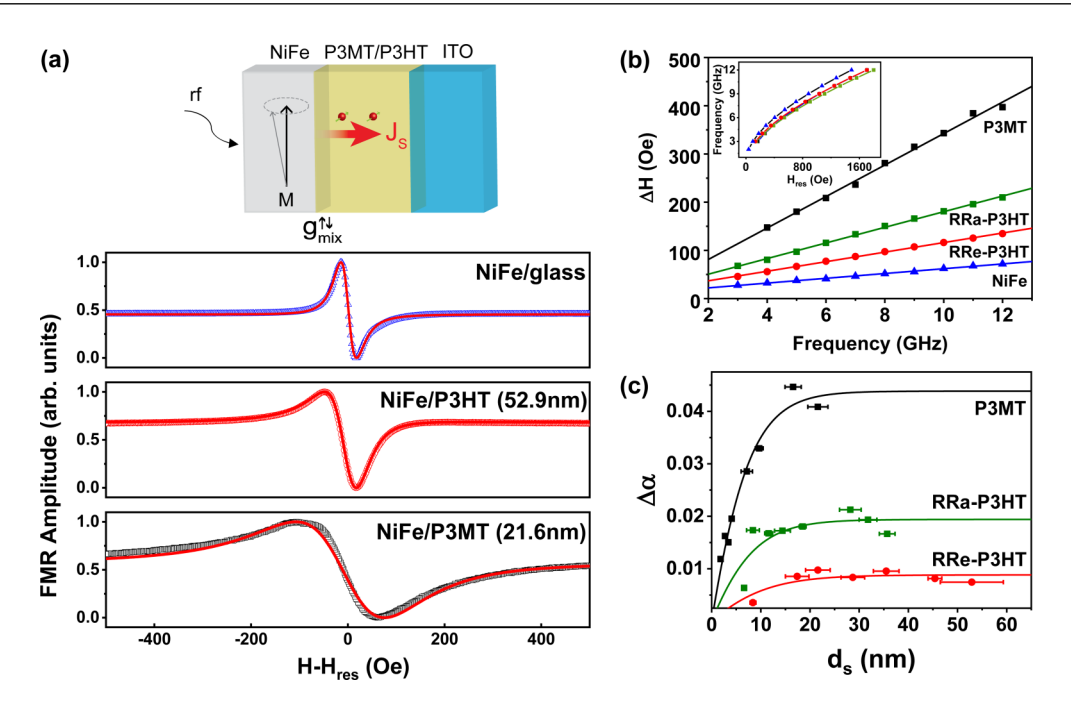


FIG. 2. (a) Schematic representation of spin pumping during FMR and typical FMR spectra normalized by the resonant field (H_{res}) obtained at 9 GHz for Ni₈₁Fe₁₉/glass, Ni₈₁Fe₁₉/RRe-P3HT(52.9 nm)/ITO, and Ni₈₁Fe₁₉/P3MT(21.6 nm)/ITO. (b) FMR linewidth (HWHM) versus microwave frequency for samples shown in (a), as well as RRa-P3HT, with linear fits for the derivation of the respective damping parameters. Inset shows microwave frequency plotted as a function of resonant field and associated fits to the Kittel equation [Eq. (2)]. (c) $\Delta \alpha$ plotted as a function of thickness for P3MT, RRe-P3HT, and RRa-P3HT series.

 $10^{19} \,\mathrm{m}^{-2}$). Whereas the obtained spin-diffusion lengths in both films are reasonable and consistent with most organic materials, the obtained spin-mixing conductances, $g_{\mathrm{eff}}^{\uparrow\downarrow}$ and $g^{\uparrow\downarrow}$, in the P3MT are surprisingly two orders of magnitude higher than that in the conventional metallic and semiconductor systems (in the range of 10^{18} to $10^{19} \,\mathrm{m}^{-2}$) despite containing predominantly light elements (i.e., mostly C and S in the polymer, minor amounts of Br, P, and O in the polymer and monolayer). This indicates an intensive spin-current injection from the NiFe layer into the P3MT polymer (the injected spin-current density at the interface, $J_S^0 \propto \frac{g_{\mathrm{eff}}^{\uparrow\uparrow} \gamma^2 h^2}{\alpha^2}$, where γ is the gyromagnetic ratio, h is the B_1 -field component of the microwave excitation [12]), which is consistent with the enhanced electrical spin injection demonstrated previously in organic spin valves using P3MT polymer brushes [27].

B. ISHE measurement

ISHE measurements were performed in a similar measurement setup used for FMR at room temperature. A sketch of the device structure used for the ISHE experiment is shown in Fig. 3(a). The pure spin current generated by the microwave dissipates into the polymer layer at the resonance field of FMR. By transmitting across the polymer spacer layer, the pure spin current (J_s) is converted into a transverse electric field (E_{ISHE}) via the inverse spin Hall effect in the ITO electrode [28]: $E_{ISHE} = \theta_{ISHE}J_s \times S$, where θ_{ISHE} is the spin Hall angle in the spin-to-charge converter (i.e., ITO electrode in this case) and S is the spin-polarization vector in the J_s along with the magnetization direction of the NiFe layer. We assume negligible spin-to-charge conversion occurring in the organic

layers $[\theta_{ISHE}(\text{polymer}) \ll \theta_{ISHE}(\text{ITO})]$. The measured voltage is generated from the ITO layer, with a spin Hall angle on the order of $\theta_{ISHE}(\text{ITO}) = 0.0065$ [29], which dominates the ISHE response. Consequently, this trilayer device is used as a sensitive detector of spin transport in the polymer film, thereby allowing for the facile extraction of the spin-diffusion length, λ_s , in both P3MT and P3HT films.

Figures 3(b) and 3(c) show typical spectra of the acquired voltage as a function of the applied magnetic field, obtained for different microwave excitation powers. The voltage signal can be decomposed into two parts, a symmetric and an antisymmetric voltage contribution given by $V(H) = V_0 + V_{\text{Sym}} \frac{\Delta H^2}{(H - H_{FMR})^2 + \Delta H^2} - V_{Asym} \frac{\Delta H(H - H_{FMR})}{(H - H_{FMR})^2 + \Delta H^2}$, where V_{Sym} is the voltage contribution stemming from the ISHE contribution in the ITO layer and V_{Asym} is the anomalous Hall-effect (AHE) contribution from the NiFe layer [12]. Flipping of the voltage polarity with reversal of the applied magnetic field from $+H_{res}$ to $-H_{res}$ provides strong evidence that the signal is indeed originating from the ISHE process. Here, we take the average of V_{Sym} for $+H_{\text{res}}$ and $-H_{\text{res}}$ as the actual V_{ISHE} , where $V_{ISHE} = [V_{Sym}(+H_{res}) - V_{Sym}(-H_{res})]/2$. Insets in Figs. 3(b) and 3(c) show the linear dependence of the extracted V_{ISHE} as a function of applied microwave power. These tendencies are consistent with the expected behaviors of V_{ISHE} induced by the spin pumping and cancel out the possible thermal-induced ordinary Seebeck contribution that is field independent [30].

Figures 3(d)-3(f) show the exponential decay behavior of V_{ISHE} as a function of organic layer thickness (d_s) , which exhibits the expected monotonic decrease owing to the spin-current transmission across the organic spacer layer between the ferromagnet and the spin sink [13]. By fitting the

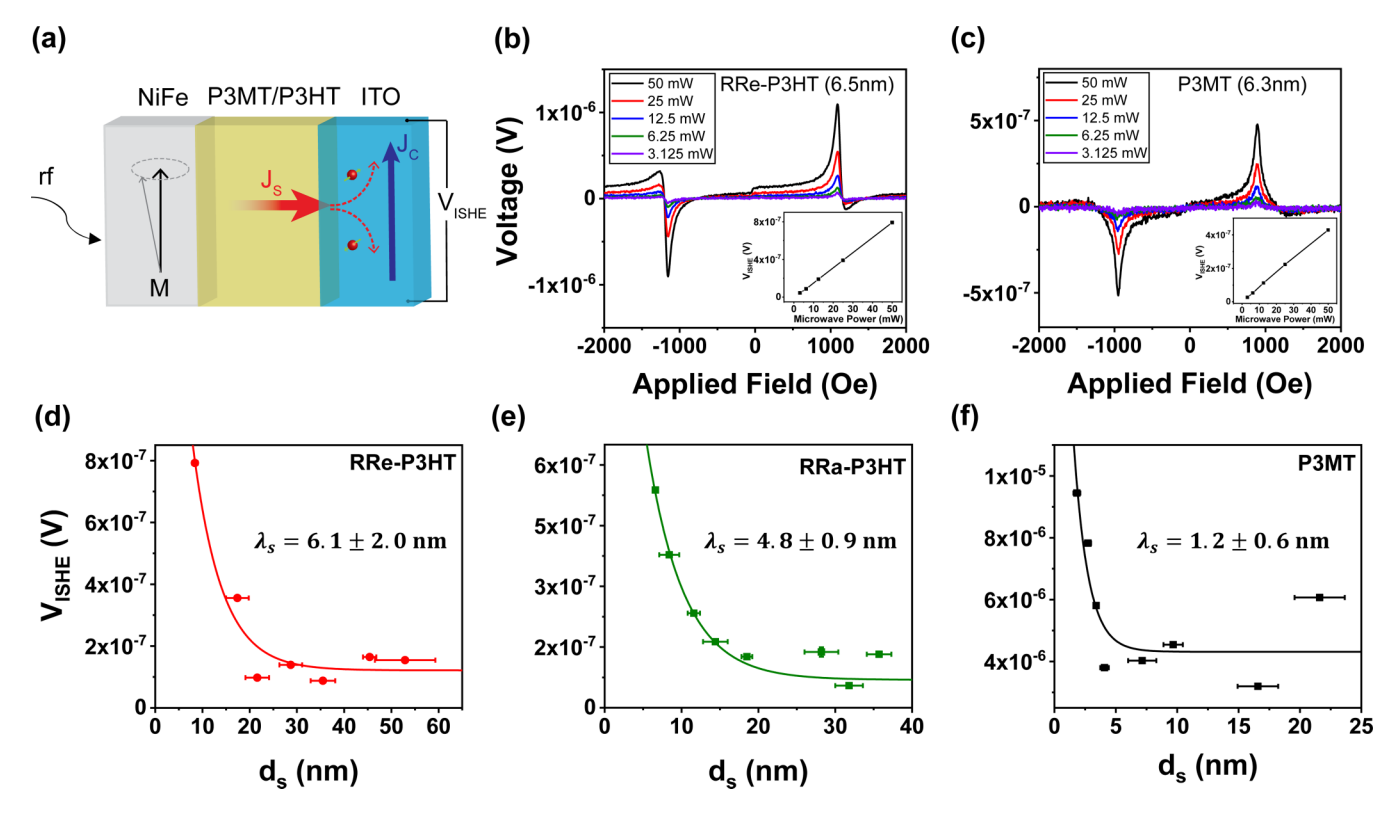


FIG. 3. (a) Schematic representation of ISHE measurements. Total voltage containing both symmetric and antisymmetric contributions measured as a function of applied field for different microwave excitation powers at a frequency of 9 GHz is shown for (b) RRe-P3HT (6.5 nm) and (c) P3MT (6.3 nm), with insets showing the linear dependence of the extracted ISHE voltage (symmetric voltage contribution) versus microwave power. ISHE voltage plotted as a function of organic layer thickness is shown for (d) RRe-P3HT, (e) RRa-P3HT, and (f) P3MT, where the fitting curves represent a simple exponential decay function with $V_{ISHE} \propto V_0 e^{\frac{-d_s}{\lambda_3}}$.

voltage thickness dependence to the exponential decay function, where $V_{ISHE}(d_s) \propto V_0 e^{\frac{-d_s}{\lambda_s}}$, we obtain values for the spin-diffusion length, $\lambda_s = 1.2 \pm 0.6$ nm in the P3MT layer at 300 K. Despite the P3MT having a higher conductivity than the P3HT layer ($\sigma_{RReP3HT} \sim 1 \times 10^{-7}$ S/cm $< \sigma_{P3MT} \sim 7 \times 10^{-6}$ S/cm) [25,31], a longer spin-diffusion length is obtained in the P3HT layer, with $\lambda_s = 6.1 \pm 2.0$ nm for RRe-P3HT and $\lambda_s = 4.8 \pm 0.9$ nm for RRa-P3HT. The P3MT layer has a consistently shorter spin-diffusion length compared to that of the P3HT layer, in line with the results extracted from the FMR measurement ($\lambda_s \approx 15$ nm for RRe-P3HT and ≈ 10 nm for P3MT).

It should be noted here that for spin pumping into organic materials, while the mechanism of spin-current generation from FMR in the ferromagnetic thin film remains the same, there are key differences in the subsequent transmission of the spin current across the ferromagnet/organic interface, and in spin-to-charge conversion as it relates to the ISHE. Whereas in metallic systems and highly doped inorganic semiconductors spin transport is mediated primarily by free carriers, in organic semiconductors it is instead polarons that mediate spin transport as supported by spin-pumping experiments performed in both local measurements using a vertical trilayer system [13] and nonlocal measurements using a horizontal configuration [22]. A caveat to this is in highly doped conjugated polymers, where a sufficiently high spin density ($\sim 10^{20} \, \mathrm{cm}^{-3}$) results in an exchange-based spin-diffusion regime allowing for the

decoupling of spin and charge transport [22]. This is evidenced in the extracted λ_s of our undoped RRe-P3HT, which is two orders of magnitude shorter than the reported value in F4TCNQ-doped P3HT (>550 nm) [22]. A much lower conductivity and spin density in our undoped P3HT may greatly suppress the spin-diffusion length, with spin transport mediated predominantly by polarons.

C. Theoretical model

There are two key findings from the results of the FMR and ISHE measurements. First, P3MT polymer brushes exhibit a shorter spin-diffusion length and higher effective damping (i.e., spin-mixing conductance) than that of P3HT films. The very short spin-diffusion length (<2 nm) suggests an additional spin-orbit coupling contribution in the P3MT polymer brushes despite it containing the same elements with low atomic number as that in P3HT films with comparable hyperfine interaction. Second, the spin-diffusion length obtained from fitting of the FMR data based on the spinbackflow model is inconsistent with, and much larger than, that obtained through ISHE response with almost an order of magnitude variation in the case of P3MT (1.2 vs 10.0 nm). This discrepancy has been observed in ISHE devices based on inorganic semiconductors such as in metal-silicon-metal vertical structures [32]. To address these two points, we need to revisit the origins of SOC in conjugated polymers. We

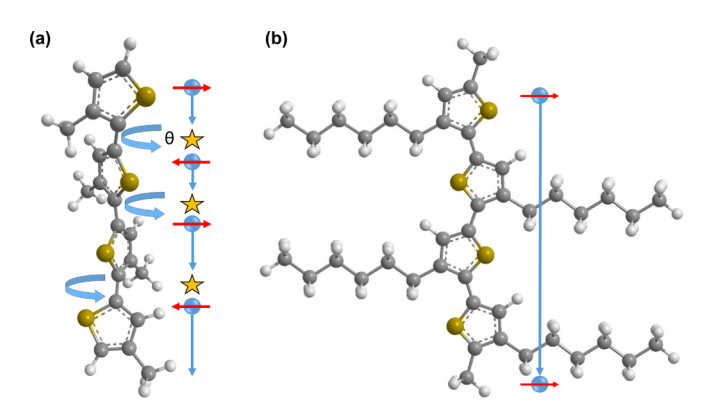


FIG. 4. Schematic representations of (a) P3MT in which the thiophene backbone is twisted by an angle θ and (b) RRe-P3HT in a planar configuration. Blue spheres and red arrows represent electrons and their spin-polarization direction, respectively, with spin-flip scattering events located at torsion sites in the case of P3MT.

note that the conventional spin-pumping model, originally developed for metals, does not consider the heterogeneous interface and junction nor the band alignment between metals and organic semiconductors. Thus we next examine whether these equations used to derive the aforementioned parameters can be appropriately applied to our case with reasonable modifications.

Spin-orbit coupling in polymers

The origins of the SOC in organic materials have been examined theoretically [18]. It was found that, in comparison to inorganic systems, the SOC in disordered organic materials for spintronics can be conveniently characterized by a dimensionless spin-mixing parameter γ , and that the spin-diffusion length can be expressed concisely as

$$\lambda = \frac{R}{4\gamma},\tag{3}$$

where R is the carrier hopping distance. For sexithiophene (T_6) , which is a typical planar system comparable to the conjugated thiophene backbone of P3HT and P3MT, y for electrons is $\sim 6.7 \times 10^{-3}$ [19]. Using this value along with a reported hopping distance $R = 0.38 \,\mathrm{nm}$ for P3HT [33,34], we obtain a spin-diffusion length of $\lambda = 14.2 \,\mathrm{nm}$ for P3HT. For P3MT, we must also consider the effect of the polymers' structural conformation on γ . P3HT has a relatively planar lamellar morphology, where polymer chains lie in the plane of the film with vertically oriented π - π stacking between adjacent chains [Fig. 4(b)]. The P3MT polymer brushes, on the other hand, are oriented vertically out of the film plane and possess a significant torsion angle between repeat units due to the nature of the growth method [Fig. 4(a)], causing shorter average conjugation in P3MT and a blueshift in the P3MT absorbance spectrum compared to P3HT as seen in Fig. 1(g) [24]. The effect of torsion on the spin-mixing parameter γ can be expressed as

$$\gamma^2 = \gamma_0^2 (1 + \alpha \tan^2 \theta), \tag{4}$$

where γ_0^2 is the SOC of the planar structure, θ is the torsion angle, and α is a numerical constant ranging from 0.135 to 0.5

according to modeling of biphenyl. As θ approaches 90°, and the π orbitals of the conjugated system are increasingly misaligned, γ^2 increases sharply. This structural conformational dependence of the SOC has been previously employed to explain the abnormally large SOC in Alq₃ molecules despite its lack of heavy elements, due to the nearly orthogonal relationship between aromatic ligands in the molecule [19]. By considering an example of a torsion angle for P3MT of $\theta=65^\circ$, with $\alpha=0.16$ and $\gamma_0=6.7\times10^{-3}$, γ would be increased from 6.7×10^{-3} to 8.9×10^{-3} , resulting in a decrease of the spin-diffusion length from 14.2 nm (calculated for the planar P3HT) to 10.7 nm (calculated for the twisted P3MT).

In addition, given constant but distinct SOCs for P3HT and P3MT, we would expect the FMR damping parameter for both polymers to saturate above a certain film thickness. Saturation of $\Delta \alpha$ is clearly observed with spin-cast P3HT films thicker than \sim 20 nm, but not in the thickness range of measured P3MT films [Fig. 2(c)]. There are at least two possible explanations for nonsaturating $\Delta \alpha$ behavior for P3MT: (i) saturation occurs in P3MT films thicker than can be measured with the experimental setup used here, or (ii) the SOC in P3MT changes with thickness. As noted previously, P3MT films possess more and more short conjugation units as they grow, evidenced by an increasingly strong blueshifted feature in their absorbance spectra [25]. An increase in the prevalence of short conjugation units in P3MT films may in turn cause an increase in the SOC with thickness and the observed nonsaturating behavior in $\Delta \alpha$. In contrast, presynthesized P3HT has an average conjugation length that is primarily determined before film deposition, yielding a constant SOC with film thickness.

IV. CONCLUSION

FMR and ISHE measurements of P3MT polymer brushes and spin-cast P3HT films showed that the former has a significant enhancement in spin-mixing conductance and reduction in spin-diffusion length compared with the latter, despite their similar chemical structures. We attribute the observed large increase in damping with increasing P3MT film thickness to a torsion-induced SOC, based on a model of spin pumping in disordered organic semiconductors. This study offers a route for intrinsically tailoring SOC in organic semiconductors and achieving efficient spin injection for future spin-to-charge converter applications through manipulation of the structural conformation of conjugated polymers.

ACKNOWLEDGMENTS

E.V. and D.S. are grateful for support from the startup funds provided by North Carolina State University and National Science Foundation Grant No. ECCS 1933297. Z.-G.Y was supported by the U. S. Army Research Office under Contract No. W911NF-17-1-0511. I.V.W. was supported by the National Science Foundation Graduate Research Fellowship under Grant No. DGE-1650116. I.V.W and W.Y. were supported by NSF Grant No. DMR-1610879. Parts of this work were performed in part at the Chapel Hill Analytical and Nanofabrication Laboratory, CHANL, a member of the

North Carolina Research Triangle Nanotechnology Network, RTNN, which is supported by the National Science Foundation, Grant No. ECCS-1542015, as part of the National Nanotechnology Coordinated Infrastructure, NNCI. D.K. acknowledges support from the National Science Foundation (Grant No. DMR-1751455).

D.S. and W.Y. conceived this study and the experiment. E.V., I.V.W., and L.Y. fabricated the devices. E.V. and S.Y.

measured the FMR, spin pumping, and calibrated rf field. I.V.W. measured the AFM and x-ray diffraction. S.K. and D.K. assisted in sample preparation. Z.-G.Y. provided the theoretical model. E.V., I.V.W., and D.S. wrote the text. D.S. and W.Y. were responsible for the project planning and group managing. All authors discussed the results, worked on data analysis, and manuscript preparation.

The authors declare no competing financial interest.

- [1] S. A. Wolf, D. D. Awschalom, R. A. Buhrman, J. M. Daughton, S. von Molnár, M. L. Roukes, A. Y. Chtchelkanova, and D. M. Treger, Science 294, 1488 (2001).
- [2] S. D. Bader and S. S. P. Parkin, Annu. Rev. Condens. Matter Phys. 1, 71 (2010).
- [3] H. Nakayama, K. Ando, K. Harii, T. Yoshino, R. Takahashi, Y. Kajiwara, K. Uchida, Y. Fujikawa, and E. Saitoh, Phys. Rev. B. 85, 144408 (2012).
- [4] Q. Song, H. Zhang, T. Su, W. Yuan, Y. Chen, W. Xing, J. Shi, J. Sun, and W. Han, Sci. Adv. 3, e1602312 (2017).
- [5] S. Zhang and A. Fert, Phys. Rev. B 94, 184423 (2016).
- [6] K. Ando and E. Saitoh, Nat. Commun. 3, 629 (2012).
- [7] H. Tetlow and M. Gradhand, Phys. Rev. B. 87, 075206 (2013).
- [8] Y. Niimi, M. Morota, D. H. Wei, C. Deranlot, M. Basletic, A. Hamzic, A. Fert, and Y. Otani, Phys. Rev. Lett. 106, 126601 (2011).
- [9] J. C. Rojas Sánchez, L. Vila, G. Desfonds, S. Gambarelli, J. P. Attané, J. M. De Teresa, C. Magén, and A. Fert, Nat. Commun. 4, 2944 (2013).
- [10] M. Jamali, J. S. Lee, J. S. Jeong, F. Mahfouzi, Y. Lv, Z. Zhao, B. K. Nikolić, K. A. Mkhoyan, N. Samarth, and J. P. Wang, Nano Lett. 15, 7126 (2015).
- [11] O. Mosendz, J. E. Pearson, F. Y. Fradin, G. E. W. Bauer, S. D. Bader, and A. Hoffmann, Phys. Rev. Lett. 104, 046601 (2010).
- [12] K. Ando, S. Takahashi, J. Ieda, Y. Kajiwara, H. Nakayama, T. Yoshino, K. Harii, Y. Fujikawa, M. Matsuo, S. Maekawa, and E. Saitoh, J. Appl. Phys. 109, 103913 (2011).
- [13] S. Watanabe, K. Ando, K. Kang, S. Mooser, Y. Vaynzof, H. Kurebayashi, E. Saitoh, and H. Sirringhaus, Nat. Phys. 10, 308 (2014).
- [14] K. Ando, S. Watanabe, S. Mooser, E. Saitoh, and H. Sirringhaus, Nat. Mater. 12, 622 (2013).
- [15] J. B. S. Mendes, O. Alves Santos, J. P. Gomes, H. S. Assis, J. F. Felix, R. L. Rodríguez-Suárez, S. M. Rezende, and A. Azevedo, Phys. Rev. B. 95, 014413 (2017).
- [16] D. Sun, K. J. van Schooten, M. Kavand, H. Malissa, C. Zhang, M. Groesbeck, C. Boehme, and Z. Valy Vardeny, Nat. Mater. 15, 863 (2016).
- [17] L. Nuccio, M. Willis, L. Schulz, S. Fratini, F. Messina, M. D'Amico, F. L. Pratt, J. S. Lord, I. McKenzie, M. Loth, B. Purushothaman, J. Anthony, M. Heeney, R. M. Wilson, I. Hernández, M. Cannas, K. Sedlak, T. Kreouzis, W. P. Gillin, C. Bernhard, and A. J. Drew, Phys. Rev. Lett. 110, 216602 (2013).
- [18] Z. G. Yu, Phys. Rev. Lett. 106, 106602 (2011).
- [19] Z. G. Yu, Phys. Rev. B. 85, 115201 (2012).
- [20] H. Liu, J. Wang, M. Groesbeck, X. Pan, C. Zhang, and Z. Valy Vardeny, J. Mater. Chem. C 6, 3621 (2018).

- [21] S. Liang, R. Geng, B. Yang, W. Zhao, R. C. Subedi, X. Li, X. Han, and T. D. Nguyen, Sci. Rep. 6, 19461 (2016).
- [22] S. J. Wang, D. Venkateshvaran, M. R. Mahani, U. Chopra, E. R. McNellis, R. Di Pietro, S. Schott, A. Wittmann, G. Schweicher, M. Cubukcu, K. Kang, R. Carey, T. J. Wagner, J. N. M. Siebrecht, D. P. G. H. Wong, I. E. Jacobs, R. O. Aboljadayel, A. Ionescu, S. A. Egorov, S. Mueller, O. Zadvorna, P. Skalski, C. Jellett, M. Little, A. Marks, I. McCulloch, J. Wunderlich, J. Sinova, and H. Sirringhaus, Nat. Electron. 2, 98 (2019).
- [23] A. Wittmann, G. Schweicher, K. Broch, J. Novak, V. Lami, D. Cornil, E. R. McNellis, O. Zadvorna, D. Venkateshvaran, K. Takimiya, Y. H. Geerts, J. Cornil, Y. Vaynzof, J. Sinova, S. Watanabe, and H. Sirringhaus, Phys. Rev. Lett. 124, 027204 (2020).
- [24] See Supplemental Material at http://link.aps.org/supplemental/ 10.1103/PhysRevMaterials.4.085603 for extended experimental methods and details, comments on repeatability, and brief discussions regarding spin pumping in trilayer structures and torsion angles in polyalkylthiophenes, see Refs. [35–45].
- [25] I. A. VonWald, M. M. Moog, T. W. LaJoie, J. D. Yablonski, D. M. DeLongchamp, J. Locklin, F. Tsui, and W. You, J. Phys. Chem. C 122, 7586 (2018).
- [26] C. Kittel, Phys. Rev. 73, 155 (1948).
- [27] R. Geng, A. Roy, W. Zhao, R. C. Subedi, X. Li, J. Locklin, and T. D. Nguyen, Adv. Funct. Mater. **26**, 3999 (2016).
- [28] E. Saitoh, M. Ueda, and H. Miyajima, Appl. Phys. Lett. **88**, 182509 (2006).
- [29] Z. Qiu, T. An, K. Uchida, D. Hou, Y. Shiomi, Y. Fujikawa, and E. Saitoh, Appl. Phys. Lett. 103, 182404 (2013).
- [30] F. L. Bakker, A. Slachter, J.-P. Adam, and B. J. van Wees, Phys. Rev. Lett. 105, 136601 (2010).
- [31] A. N. Caruso, D.-Q. Feng, Ya. B. Losovyj, D. L. Schulz, S. Balaz, L. G. Rosa, A. Sokolov, B. Doudin, and P. A. Dowben, Phys. Status Solidi Basic Res. 243, 1321 (2006).
- [32] C. Cerqueira, J. Y. Qin, H. Dang, A. Djeffal, J.-C. Le Breton, M. Hehn, J.-C. Rojas-Sanchez, X. Devaux, S. Suire, S. Migot, P. Schieffer, J.-G. Mussot, P. Łaczkowski, A. Anane, S. Petit-Watelot, M. Stoffel, S. Mangin, Z. Liu, B. W. Cheng, X. F. Han, H. Jaffrès, J.-M. George, and Y. Lu, Nano Lett. 19, 90 (2019).
- [33] N. Kleinheinz, N. Persson, Z. Xue, P. H. Chu, G. Wang, Z. Yuan, M. A. McBride, D. Choi, M. A. Grover, and E. Reichmanis, Chem. Mater. 28, 3905 (2016).
- [34] J. D. Roehling, I. Arslan, and A. J. Moulé, J. Mater. Chem. 22, 2498 (2012).
- [35] W. R. Salaneck, O. Inganäs, B. Thémans, J. O. Nilsson, and B. Sjögren, J. Chem. Phys. 89, 4613 (1988).
- [36] S. B. Darling and M. Sternberg, J. Phys. Chem. B 113, 6215 (2009).

- [37] S. Hotta and K. Ito, in *Handbook of Oligo- and Polythiophenes*, edited by D. Fichou (Wiley-VCH, 1999). Vol. 1, pp. 45–82.
- [38] R. S. Bhatta and D. S. Perry, Comput. Theor. Chem. **1008**, 90 (2013).
- [39] A. Bongini and A. Bottonio, J. Phys. Chem. A 103, 6800 (1999).
- [40] S. S. Zade and M. Bendikov, Chem. A Eur. J. 13, 3688 (2007).
- [41] G. Caple, B. L. Wheeler, R. Swift, T. L. Porter, and S. Jeffers, J. Phys. Chem. 94, 5639 (1990).
- [42] D. Alberga, A. Perrier, I. Ciofini, G. F. Mangiatordi, G. Lattanzi, and C. Adamo, Phys. Chem. Chem. Phys. 17, 18742 (2015).
- [43] M. Böckmann, T. Schemme, D. H. de Jong, C. Denz, A. Heuer, and N. L. Doltsinis, Phys. Chem. Chem. Phys. 17, 28616 (2015).
- [44] V. Hernandez, F. J. Ramirez, T. F. Otero, and J. T. Lopez Navarrete, J. Chem. Phys. 100, 114 (1994).
- [45] V. Hernandez and J. T. Lopez Navarrete, J. Chem. Phys. 101, 1369 (1994).